CALIBRATING PREDICTIONS OF FAULT SEAL REACTIVATION IN THE TIMOR SEA

S.D. Mildren, R.R. Hillis and J.Kaldi
National Centre for Petroleum Geology and Geophysics
and Australian Petroleum Cooperative Research Centre
Thebarton Campus
University of Adelaide SA 5005
smildren@ncpgg.adelaide.edu.au

ABSTRACT

Predictions of the likelihood of fault reactivation for five fault-bound prospects in the Timor Sea are made using the FAST (Fault Analysis Seal Technology) technique. Fault reactivation is believed to be the dominant cause of seal breach in the area. Calculations are made using a stress tensor appropriate for the area, a conservative fault-rock failure envelope and the structural geometries of each prospect. A depth-stress power relationship defines the vertical stress magnitude based on vertical stress profiles for 17 Timor Sea wells.

Empirical evidence of hydrocarbon leakage at each trap is used to investigate the accuracy of the fault reactivation-based predictions of seal integrity. There is a good correlation between evidence of leakage and the risk of reactivation predicted using the FAST technique. Risk of reactivation is expressed as the pore pressure increase (ΔP) that would be required to induce failure. This study allows the fault reactivation predictions to be calibrated in terms of risk of seal breach. Low integrity traps are associated with ΔP values less than 10 MPa, moderate integrity traps correspond with values between 10 and 15 MPa and high integrity traps correspond with values greater than 15 MPa. Faults with dip magnitudes greater than 60° in the Timor Sea area are likely to have a high risk of reactivation and shear failure is the most likely mode of reactivation.

KEYWORDS

FAST, fault reactivation, in situ stress, trap integrity

INTRODUCTION

The integrity of structurally-bound hydrocarbon traps is dictated by the sealing potential of their caprocks and bounding faults. Both caprocks and the faults can be breached by several failure mechanisms including membrane failure, fault juxtaposition and dynamic reactivation (Watts, 1987; Jones et al, 2000). FAST (Fault Analysis Seal Technology) mapping is an innovative new technique for assessing the risk associated with hydraulic or dynamic failure/reactivation of faults in terms of the contemporary stress field. This technique was originally introduced by Jones et al (2000). The fundamental risk calculation algorithm, however, has been improved and is described within this paper. Despite the rapidly growing use of this technique, there has never been a detailed comparison of FAST predictions to exploration results.

Contemporary hydrocarbon leakage in the Bonaparte Basin is recognised to be closely associated with faults (e.g. Whibley and Jacobsen, 1990; O'Brien and Woods, 1995). Caprock lithologies are believed to be thick and regionally extensive suggesting that fault juxtaposition is not a dominant failure mechanism. Capillary pressures of the regional seals are very high and seal failure due to capillary leakage is unlikely (Kivior et al, 2002). In addition, there exists an extensive body of empirical evidence demonstrating fault related hydrocarbon leakage across the Bonaparte Basin (Lisk et al, 1998; O'Brien et al, 1998; O'Brien and Woods, 1995).

Although it is widely accepted that Late Miocene to Recent reactivation of faults is a major seal integrity issue in the Timor Sea, the nature of the relationship between seal breach and faults is not completely understood. Kinematic approaches suggest that leakage is associated with the angular relationship between Tertiary and Mesozoic faults (O'Brien and Woods, 1995) or by faulting associated with soft-link relay ramps during Tertiary extension (Cooper et al, 1998). Although not disregarding kinematic approaches to problems of these types, it is important to consider the dynamic (stress) environment of faults independent of their origin and age. The FAST technique integrates structural geometries with the contemporary in situ stress field and fault-rock properties to assess fault reactivation risk in this manner. Fault reactivation is believed to cause seal breach and there is abundant evidence that at stresses close to failure, faults transmit fluids (Sibson, 1996; Barton et al, 1995).

This paper describes the FAST technique used to estimate contemporary fault reactivation and calculates reactivation risk for five structurally bound fields/ prospects in the Timor Sea. Risk maps are generated using a generalised stress tensor and failure envelope for the region.

A large amount of empirical data indicating the seal integrity of each of these structures has been acquired over the last 10 years. These data are compared to the geometrically-based predictions of the FAST technique, and in turn are used to calibrate the risk values provided by FAST for use elsewhere in the Timor Sea. Use of the generalised stress tensor and rock properties is justified by the correlation between FAST predictions and evidence of seal breach and enables quick, but reliable, assessments of dynamic fault seal integrity to be made across the Timor Sea. Where appropriate, regional analysis of the type presented here can be followed up by more detailed analysis using, for example, fault maps

from 3D seismic data, in situ stress data and rock strength estimates from the specific prospect.

EVIDENCE OF TRAP INTEGRITY

Five structurally-bound traps were selected on the basis of the availability of published data from which to assess their seal integrity remotely. These are: Challis, East Swan, Elang, Oliver and Skua (O'Brien and Woods, 1995; O'Brien et al, 1996; Lisk et al, 1998; O'Brien et al, 1998; Cowley and O'Brien, 2000). The empirical evidence for hydrocarbon leakage are based on the following analyses.

Airborne Laser Fluorescence (ALF) remotely identifies contemporary hydrocarbon slicks on the oceans surface using an ultra-violet laser (Martin and Cawley, 1991; O'Brien et al, 1998).

Geochemical sniffer surveys sample contemporary hydrocarbon content in ocean bottom waters by means of tool towed below a moving ship (O'Brien et al, 1992; O'Brien et al, 1998).

Hydrocarbon related diagenetic zones (HRDZs) are areas where oxidation of leaked hydrocarbons has resulted in the precipitation of diagenetic carbonate cement in aquifer sands. The acoustic impedence of the diagenetic zones is such that a strong response is observed on seismic sections (O'Brien and Woods, 1995; Cowley and O'Brien, 2000).

Fluid inclusion analyses (GOI) enables the identification of palaeo oil columns based on the percentage of fluid inclusions containing oil (Lisk and Eadington, 1994; Lisk et al, 1998).

The data pertinent to the five structures assessed in this study are summarised in Table 1.

The Challis structure

The Challis Field is bound to the north by a northeast striking fault and covers an area of approx 7 km². The structural spill point is located in the northeast sector of the field (Wormald, 1988). Fluid inclusion analyses suggest that no significant residual oil column underlies the live column at Challis–1 (Lisk et al, 1998). Oil shows were observed, however, below the present free water level (FWL) in all Challis wells up to Challis–5, which had the thickest interval of 59 m (Wormald, 1988). The Challis Field is believed to be the only oil field in the Timor sea that does not have associated HRDZ (O'Brien et al, 1996). Trap integrity of the Challis Field is hence classified as moderate to high.

East Swan structure

The East Swan structure is located on the southeast margin of the Swan Graben. No live hydrocarbon columns were identified in either East Swan–1 or East Swan–2 although residual columns are present (O'Brien et al, 1996; Lisk et al, 1998). A prominent band of ALF anomalies 5 km wide and 17 km long exists SW of the East Swan

Table 1. Summary of empirical evidence used to classify trap integrity. Lat and Long are latitude and longitude, HC Column Height is the height of the live hydrocarbon column encountered (in metres), FHA indicates if fluid history analysis has been performed, Residual Column is the height of the residual oil column (in metres), Sniffer Evidence indicates if a sniffer anomaly is associated with the well, ALF indicates if an ALF anomaly is associated with the well (blanks indicate no Sniffer or ALF data) and Integrity is the seal integrity of the trap indicated by that well data.

Well	Lat	Long	HC Column Height (m)	FHA	Residual Column (m)	HRDZ	Sniffer Evidence	ALF	Integrity
Challis Field									
Challis–1	-12.12	125.00	29	Y	-	N			Moderate-High
Challis–2A	-12.12	125.02	38	Y	-	N			Moderate-High
Challis–3	-12.12	125.02	37	Y	-	N			Moderate-High
Challis–4	-12.13	124.00	24	Y	-	N			Moderate-High
East Swan Prospect									
East Swan–1	-12.30	124.58	0	N	?	Y		Y	Low
East Swan–2	-12.29	124.58	0	Y	90	Y	N	Y	Low
Eclipse–1	-12.27	124.62	0	Y	215	N			Low
Elang Field									
Elang–1	-10.88	126.60	76	Y	18				Moderate-High
Elang–2	-10.88	126.59	73	N					Moderate-High
Oliver Field									
Oliver–1	-11.64	125.01	163	Y	99	N	N		High
Skua Field									
Skua–2	-12.50	124.40	9	N	?(thin)	N	Y	Y	Moderate-High
Skua–3	-12.51	124.41	47	Y	7	Y	Y	Y	Moderate-High
Skua–4ST	-12.49	124.43	51	N		N	Y	Y	Moderate-High
Swift–1	-12.54	124.45	9	Y	17	Y	Y	Y	Moderate-High

structure. A second band of anomalies is associated with the Eclipse structure NE of the East Swan wells. Sniffer data indicates generally low levels of hydrocarbons in the bottom waters although minor hydrocarbon seepage occurs close to Eclipse-1 (O'Brien at al, 1998). A massive continuous HRDZ is observed around East Swan–1 (O'Brien and Woods, 1995). Trap integrity of the East Swan structure is classified as low/breached.

Elang Field

The Elang Field is an entirely fault dependent crestal culmination on the 50 km long E–W Elang trend across the central portion of ZOCA 91-12 (Young et al, 1995). Live oil columns of 76 and 73 m were observed in Elang–1 and Elang–2 respectively. Fluid history analysis reveals high GOI values below the current FWL which indicates the presence of residual oil columns of between 10 and 18 m. Oil inclusions decorate the traces of penetrative fractures that run across several grains, suggesting flow of oil along fractures rather than infiltration through pore spaces (O'Brien et al, 1996). ALF and sniffer coverage of the Elang area is not available, and no HRDZs have been reported. Seal integrity of the Elang Structure is classified as moderate to high.

Oliver Field

The Oliver–1 well is located on the SE flank of the Cartier Trough and contains a 162.7 m gas column with a thin basal oil leg of 13–16m (O'Brien et al, 1996). The structure is filled to spill point and the presence of a 99 m palaeo-oil column within the present gas column suggests that the palaeo-column was displaced by later stage gas (O'Brien et al, 1996). A HRDZ is not observed above the trap and no ALF data exists in the area. No useful sniffer information was acquired as the hydrocarbon-detecting fish was towed too far above the sea floor (O'Brien et al, 1992). The seal integrity of the Oliver structure is classified as high.

Skua Field

The Skua structure is a tilted fault block bounded by the NE–SW striking Skua fault and located southeast of the Swan Graben. The GOI data for the Skua Field reveal the presence of a thin residual zone (10 m) below a 47 m present-day live column (O'Brien et al, 1996). No residual zone is observed on the eastern margin of the field. Sniffer surveys indicate the presence of methane and ethane concentrations adjacent to the Skua fault, which suggests active hydrocarbon seepage (O'Brien and Woods, 1995). ALF anomalies are observed around Skua with a relatively large anomaly located north of Swift–1. Evidence of small and lenticular HRDZ formation across the Skua structure is illustrated by a weak to moderate velocity anomaly in the Grebe Sands at Skua–3 and a narrow and tightly localised HRDZ over Swift–1 (O'Brien and Woods, 1995). The seal integrity of the Skua structure is classified as moderate to high.

STRUCTURAL PERMEABILITY

Structural permeability is the concept underlying the FAST methodology. The FAST methodology follows Sibson's (1996) approach to the generation of fracture-related permeability (which is itself based on fundamental brittle failure theory) and applies it to risking fault reactivation and associated seal leakage. Sibson (1996) recognises the following elements of structural permeability:
• tensile fractures;
• shear fractures; and
• mixed-mode tensile/shear fractures.

Following Sibson (1996; 1998), we assume there is a composite Griffith-Coulomb failure envelope (Fig. 1a). Assuming this failure envelope, the criteria for tensile, shear and hybrid tensile-shear reactivation may be expressed in terms of pore pressure (Table 2). These criteria apply to intact rock, or to reactivation of pre-existing faults, provided that the appropriate values of T, C and μ are used.

The differential stress $(\sigma_1 - \sigma_3)$ controls the mode of failure. If $(\sigma_1 - \sigma_3) < 4T$, tensile failure is predicted, if $4T < (\sigma_1 - \sigma_3) < 6T$ hybrid tensile-shear failure is predicted, and if $(\sigma_1 - \sigma_3) > 6T$, shear failure is predicted. If the cohesive strength of the reactivated fault zone is zero, the failure envelope passes through the origin of the normal/shear stress plot and thus reactivation in shear is the only possible mode of failure, irrespective of the differential stress.

Table 2. Failure criteria expressed in terms of pore pressure and necessary differential stress conditions for tensile, shear and hybrid tensile-shear failure assuming a composite Griffith-Coulomb failure envelope. The criteria apply to intact rock, or to reactivation of pre-existing faults/fractures, provided that the appropriate values of T, C and μ are used. Modified from Sibson (1996)

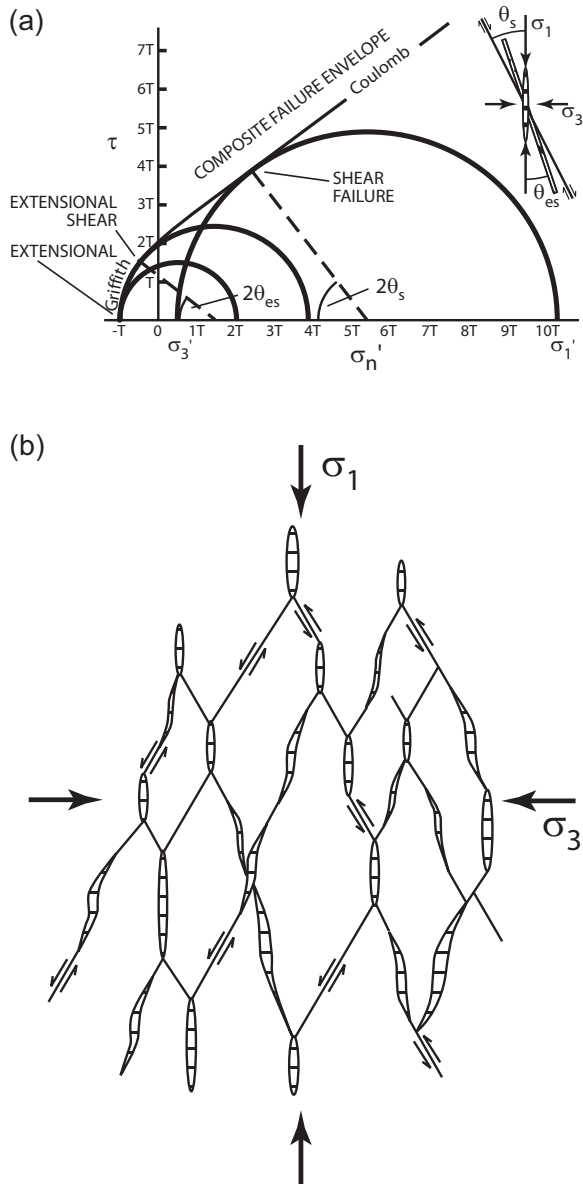| Failure Mode	Criterion	Condition
Tensile (hydraulic)	$P_p = \sigma_3 + T$	$(\sigma_1 - \sigma_3) < 4T$
Tensile/Shear	$P_p = \sigma_n + (4T^2 - \tau^2)/4T$	$4T < (\sigma_1 - \sigma_3) < 6T$
Shear	$Pp = \sigma_n + (C - \tau)/\mu$	$(\sigma_1 - \sigma_3) > 6T$

(a)

(b)

Figure 1. The elements of structural permeability: a) Mohr diagram with composite failure envelope for intact rock with tensile strength, T, illustrating the stress conditions and orientations with respect to the stress field of extensional (tensile), shear and mixed-mode (extensional-shear) failure (Sibson, 1996), and b) Network of structural permeability comprising interlinked shear, tensile and mixed-mode fractures. Diagram represents a normal fault stress regime when upright, a reverse fault stress regime when sideways, and a strike-slip regime in plan view (Sibson, 1996).

Seal failure is assessed herein in terms of the likelihood of the development of one or more of the above elements of structural permeability to provide conduits for fluid flow during reactivation (Fig. 1b). The risk of reactivation is determined using the stress tensor (Mohr Circle) and fault-rock strength (failure envelope). The risk of reactivation-related seal failure may be quantified by the increase in fluid pressure (ΔP) required to cause reactivation (Fig. 2). This is not meant to imply that failure is always due to changes in fluid pressures. However, it does provide a simple way of expressing the proximity of a plane of any given orientation (strike and dip) to the failure envelope i.e. the risk of reactivation-related seal breach.

Brittle failure is predicted if Mohr's circle touches the failure envelope. All fault orientations plot within the shaded area of the three dimensional Mohr's circle and those closest to the failure envelope are at greatest risk of reactivation (Fig. 2). The distance between each fault plane and the failure envelope indicates the increase in pore pressure (ΔP) required to cause reactivation and is used as the measure of the likelihood of fault reactivation in the FAST technique. A small ΔP infers a high likelihood of reactivation and a large ΔP infers a low likelihood of reactivation. The ΔP value for each plane can be plotted on a stereonet as poles to planes (Fig. 3). The risk of reactivation of any pre-existing fault orientation is then read from the stereonet.

A FAST map is produced by combining the reactivation risk stereonet with the fault geometry. The structural geometry can be digitally extracted for an individual seismic horizon from a seismic interpretation package. Fault polygons interpreted from seismic data are reduced to a series of centreline points. The dip and dip direction attributes are determined from the fault displacements. Alternatively, structural maps with depth contours and fault polygons can also be used. Fault dips can be
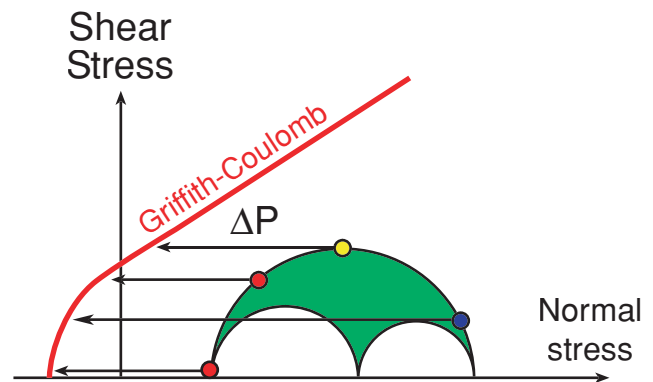

Figure 2. Three-dimensional Mohr diagram with composite Griffith-Coulomb failure envelope. All possible orientations of planes lie within the shaded area. The horizontal distance between any orientation and the failure envelope (which may be thought of as the increase in pore pressure, ΔP, required to cause failure) is used to assess the propensity of a plane to failure.
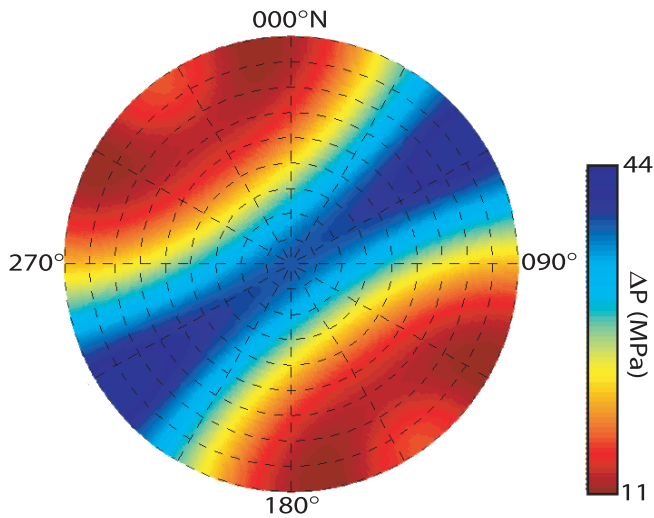
Figure 3. Likelihood of of fault/fracture plane reactivation, represented as poles to planes, for a specific stress regime and failure envelope. Numerical values on scale refer to increase in fluid pressure required to cause reactivation (ΔP). High ΔP implies low risk (blue) and low ΔP implies high risk (red). Equal angle, lower hemisphere stereographic projection of poles to planes.
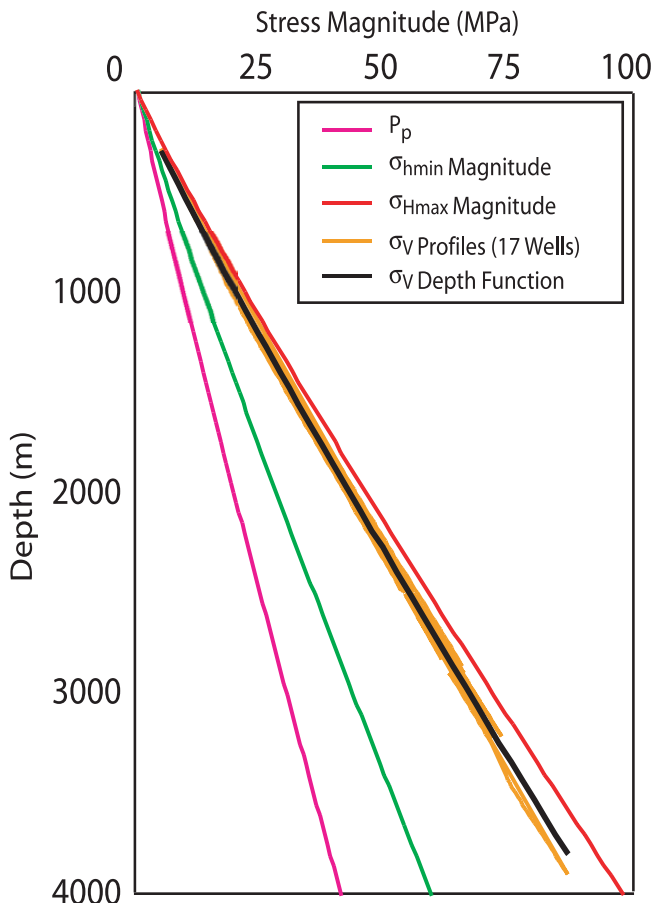

Figure 4. Generalised in situ stress tensor for the Timor Sea area.

calculated from heave and throw measurements made along strike. Both methods rely heavily on the resolution of the data and on the accuracy of the original interpretation. The risk of reactivation of each fault segment (dip, strike) is determined from the reactivation risk stereonet. The colour-coded fault segments are then plotted on a map, allowing rapid evaluation of the risk of reactivation and related fault seal breach for mapped prospects.

In order to generate fault prediction maps, three inputs are required: the in situ stress tensor, an estimate of fault rock strength and the relevant structural geometry. The following sections discuss these inputs for the Timor Sea.

BONAPARTE BASIN IN SITU STRESS TENSOR

Much work has been done to constrain the in situ stress tensor in the Timor Sea area (Hillis and Williams, 1992; Mildren et al, 1994; Hillis et al, 1997a; Hillis et al, 1997b; Castillo et al, 1998 and Hillis, 1998). With the exception of vertical stress magnitude, an amalgam of these published data have been compiled to constrain a generalised in situ stress tensor for the Timor Sea for use in this study (Fig.4). Vertical stress profiles have been calculated for 17 Timor Sea wells and are used to define a generalised depth-stress relationship for the area.

Maximum horizontal stress orientation

A considerable database of stress orientation data now exists under the banner of the Australian Stress Map (ASM) Project (Hillis and Reynolds, 2000). The ASM receives regular updates as new wells are interpreted for stress-related features. The maximum horizontal stress orientation (σ_{Hmax}) is considered to be relatively consistent across the Bonaparte Basin with the exception of measurements made in the northern parts of the ZOCA 91-01 permit area (Castillo et al, 1998; Mildren and Hillis, 2000). A mean σ_{Hmax} orientation (055°) for the Timor Sea area, excluding these anomalous orientations, has been obtained from the ASM and used in the FAST calculations.

Horizontal stress magnitudes

Hillis et al (1997b) compiled leak-off pressures from 61 wells in northern Bonaparte Basin and obtained the following expression (Equation 1) for the minimum horizontal stress magnitude.

$$\sigma_{hmin} = 0.36 (\sigma_v - Pp) + 1.0 + Pp \qquad \text{Equation 1}$$

where

σ_{hmin}	= minimum horizontal stress magnitude [MPa]
σ_v	= vertical stress magnitude [MPa]
Pp	= pore pressure [MPa].

Given that pore pressures in the region are generally at hydrostatic (hence $Pp \approx 0.45\sigma_v v$) this can be simplified to Equation 2.

$$\sigma_{hmin} \approx 0.65\sigma v \qquad \text{Equation 2}$$

The maximum horizontal stress magnitude is the most difficult component of the stress tensor to define. Seismic activity and fault-related leakage in the Timor Sea area suggest that many faults are at failure (Castillo et al, 1998; O'Brien et al, 1998). Published estimates of stress magnitudes in the Timor Sea indicate that σ_v is a lower limit to σ_{Hmax} and that the fault condition in the area lies between the boundary of normal/strike-slip and strike-slip (ie.$\sigma_{Hmax} \approx \sigma_v > \sigma_{hmin}$ to $\sigma_{Hmax} > \sigma_v > \sigma_{hmin}$; Castillo et al, 1998; Hillis, 1998). Hence, it can be assumed that the crust is at frictional equilibrium and that the σ_{Hmax} magnitude can be constrained by the frictional equilibrium relation (Equation 3; Jaeger and Cook, 1979), such that for a strike-slip stress environment:

$$\sigma_{H\max} \leq \left(\sigma_{h\min} - P_p\right)\left[\left(\mu^2+1\right)^{\frac{1}{2}}+\mu\right]^2 + P_p \qquad \text{Equation 3}$$

where

σ_{Hmax} = maximum horizontal stress magnitude
μ = the frictional coefficient.

Vertical stress magnitude

The vertical stress magnitude is calculated based on the assumption that the weight of the overburden equals the vertical stress magnitude (Equation 4; McGarr and Gay, 1978). The calculation is made using density log data acquired from hydrocarbon exploration wells.

$$\sigma_v = \int_z^0 \rho(z)g.dz \qquad \text{Equation 4}$$

where

ρ = density of the overlying rock column [gcm^{-3}]
z = depth [m]
g = acceleration due to gravity [ms^{-2}].

Density logs are not normally run from the surface, therefore vertical stress cannot be determined by simply integrating the density log data from the surface to the depth of interest. However, sonic velocity and density are strongly related. Check shot velocity survey data are used to determine average sonic velocity from the surface to the top of the density log data, and the average velocities are then converted to average densities. See Serra (1984) for details of operation of sonic and density logs and Balch and Lee (1984) for operation of check shot surveys.

Vertical stress profiles were calculated for 17 Timor Sea wells to determine a generalised stress-depth relationship for the region (Fig. 4; Table 3). A power law regression line was fitted to the dataset to derive Equation 5.

$$\sigma_v = 0.0111 \cdot Depth^{1.0878}, r^2 = 0.9985 \qquad \text{Equation 5}$$

where

r^2 = the regression coefficient.

Stress values for individual structures were calculated using Equation 5 at the average depth appropriate for the horizon of interest (Table 4).

MECHANICAL PROPERTIES OF FAULT ROCKS

One advantage of the FAST methodology is that it incorporates realistic rock strengths into the prediction of fault failure. Calculations of a similar nature such as slip tendency and dilation tendency (Ferrill et al, 1999) also make predictions of shear and tensile failure but the risk is relative, not absolute because no specific failure envelope is used. A fault may have a high slip and/or shear tendency but if the magnitude of the stresses is far removed from the strength of the rock then failure may not be an issue. For more details on the use of fault rock properties in predicting fault reactivation see Dewhurst et al (2002).

The cohesive strength of fault rocks (C) has been estimated from laboratory derived tensile strengths (T) quoted in the literature, using the approximation C~2T, as predicted by the Griffith criterion (Sibson, 1996). Dewhurst et al (2002) show that lithified cataclasites from the Otway Basin have a cohesive strength approximately 5.5 MPa and Streit (1999) suggests that cohesive strength ranges between 4–14 MPa for lithified gouges and cataclasites in general. In this study the cohesive strength has been assumed to be 5 MPa and the coefficient of friction to be 0.7. In circumstances where laboratory derived rock strengths are not available, sensitivity studies using a relevant range of strengths are recommended.

FAULT REACTIVATION PREDICTIONS

Seismic data from which to generate detailed structural geometries for each trap were not available. Prospect maps published in well completion reports and in various literature have been utilised in conjunction with depth converted geological sections to create strike and dip datasets. Where fault dip and strike were uncertain, no FAST calculations were made. Each dataset has been generated for top reservoir and utilises the appropriate in situ stress magnitudes appropriate for that depth. The predicted risk of fault reactivation is given as ΔP in MPa utilising the same scale range in all cases (0-30 MPa). The results of these calculations are illustrated in Figures 5–9.

Table 3. List of wells for which vertical stress profiles were calculated where lat and long are the latitude and longitude of the well, top and bottom are the top and bottom depths of the density log run, average sonic velocity is the average check shot velocity and average density is the Nafe-Drake transform from average check shot velocity to average density for the interval between the surface and the top of the density log.

Well Name	Lat	Long	RHOB Log Interval (m) Top	Bottom	Average Sonic Velocity (m/s)	Average Density (g/cm3)
Anderdon–1	12°38'	124°47'	2002.08	2907.80	2907	2.2
Avocet–1a	11°22'	125°46'	1191.16	2200.00	2673	2.16
Barita–1	11°26'	125°43'	1281.68	2488.54	2706	2.17
Beluga–1	11°00'	129°33'	2428.34	3083.97	2994	2.22
Bilyara–1st	12°41'	124°30'	2600.25	2838.91	3025	2.22
Brown Gannet–1	12°06'	123°51'	259.84	2733.45	1986	1.91
Challis–1	12°07'	125°00'	1194.06	1954.08	2674	2.16
Eclipse–1	12°16'	124°37'	1411.23	2987.66	2749	2.17
Fagin–1	11°34'	125°08'	2883.41	3261.36	3071	2.23
Iris–1	11°17'	126°33'	3403.09	3906.77	3146	2.24
Jabiru–1a	11°56'	125°00'	1219.05	3228.90	2683	2.16
Jabiru–2	11°56'	124°59'	1198.02	2344.98	2675	2.16
Osprey–1	12°13'	125°13'	264.57	3182.58	1994	1.92
Skua–4	12°29'	124°26'	2196.69	2652.98	2949	2.21
Swan–2	12°07'	124°18'	1555.09	3222.50	2793	2.18
Swift–1	12°32'	124°27'	1451.31	2798.22	2762	2.18
Vulcan–1b	12°09'	124°20'	1387.00	2870.61	2741	2.17

A quantitative value representing the risk of an individual trap was calculated in order to compare fault reactivation risk between traps. The maximum risk (lowest ΔP value) for each trap-bounding fault was determined. These maximum values were averaged for each trap. The maximum risk average was then compared with the empirical integrity classification (Fig. 10). Averaging reactivation risk in this manner compensates for the low resolution structural data used in this study and for variation of the geometrical relationship between bounding faults and the height of the free water level across individual traps. Where detailed structural information is available, reactivation integrity can be based on the lowest ΔP value (highest risk) within closure.

If a fault-bound trap is to be sealing it must exhibit a low risk of predicted fault-seal breach. However, the converse is not necessarily true, i.e. a trap not prone to reactivation may be non-sealing if leaking is associated with fault juxtaposition issues or where buoyancy pressure exceeds capillary pressure (caprock and/or fault). In general juxtaposition is not considered critical in the Timor Sea because throw on trap bounding faults is generally less than the thickness of the regional seal. Furthermore, capillary breakthrough pressures suggest that the regional seal can support hydrocarbon columns between 100 and 500 m high (Kivior et al, 2002). Hence fault reactivation is likely to be the key issue in the Timor Sea.

The comparison between observed trap integrity and fault reactivation predictions shows the low integrity East Swan structure to have the greatest overall risk. It is possible that this is a conservative estimate of the risk associated with the East Swan bounding fault due to the age, and therefore quality of the prospect map used to define the structural geometry (i.e. 1977). Heave and throw dip calculations estimate the fault to have considerably low dip magnitudes (<30°) along some sections. These sections contrast significantly with dip magnitudes of up to 63° along the highest risk sections of the fault. It is suspected that a recalculation of risk with updated structural information would predict lower ΔP values along some fault segments and that the overall risk for East Swan could be higher.

Challis, Skua and Elang were all classified as moderate to high integrity traps. Average maximum ΔP values range from 12 MPa (Challis and Skua) to 25 MPa (Elang), i.e. 2–15 MPa greater than the average calculated for East Swan. The predicted fault reactivation risk at Elang is considerably less than that for the high integrity Oliver trap. Indeed this is the only discrepancy between FAST predictions and observed integrity. The empirical observations on seal integrity made at Elang are based on fluid history analysis which reveals that residual columns are present and that hydrocarbons have leaked at some time from the structure. There is no clear

Table 4. Stress magnitudes used to risk fault reactivation.

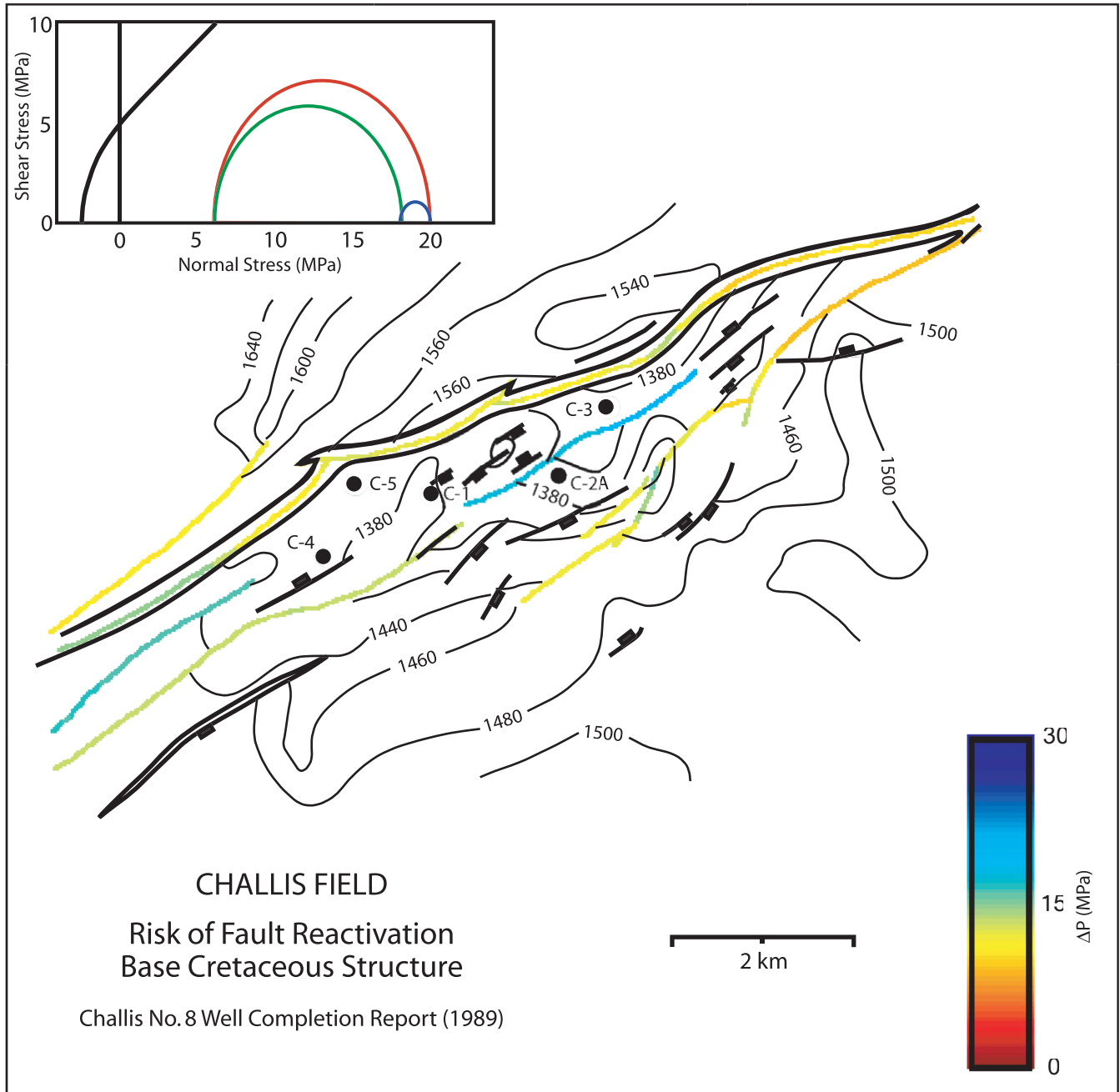| Structure	Depth (m)	P_p (MPa)	σ_v (MPa)	σ_{hmin} (MPa)	σ_{Hmax} (MPa)
Challis	1500	14	32	20	34
East Swan	2300	23	50	33	54
Elang	3000	30	67	44	72
Oliver	3300	34	75	48	80
Skua	1750	17	37	24	40

Figure 5. Predicted risk of fault reactivation for the Challis Field measured by ΔP in MPa. Three-dimensional Mohr circle (Figure insert) represents stress environment at 1,500 m depth using generalised Timor Sea stress tensor.
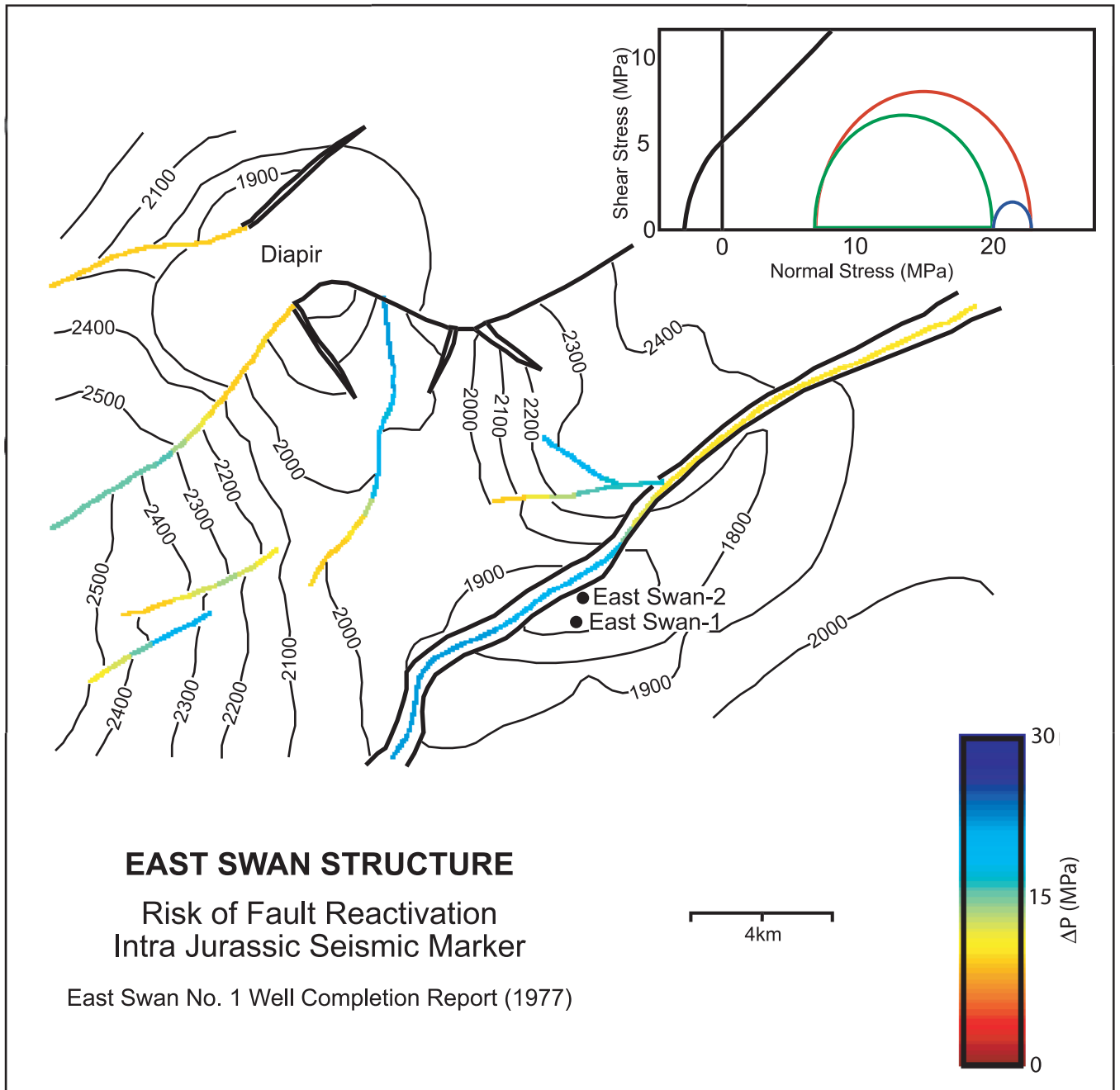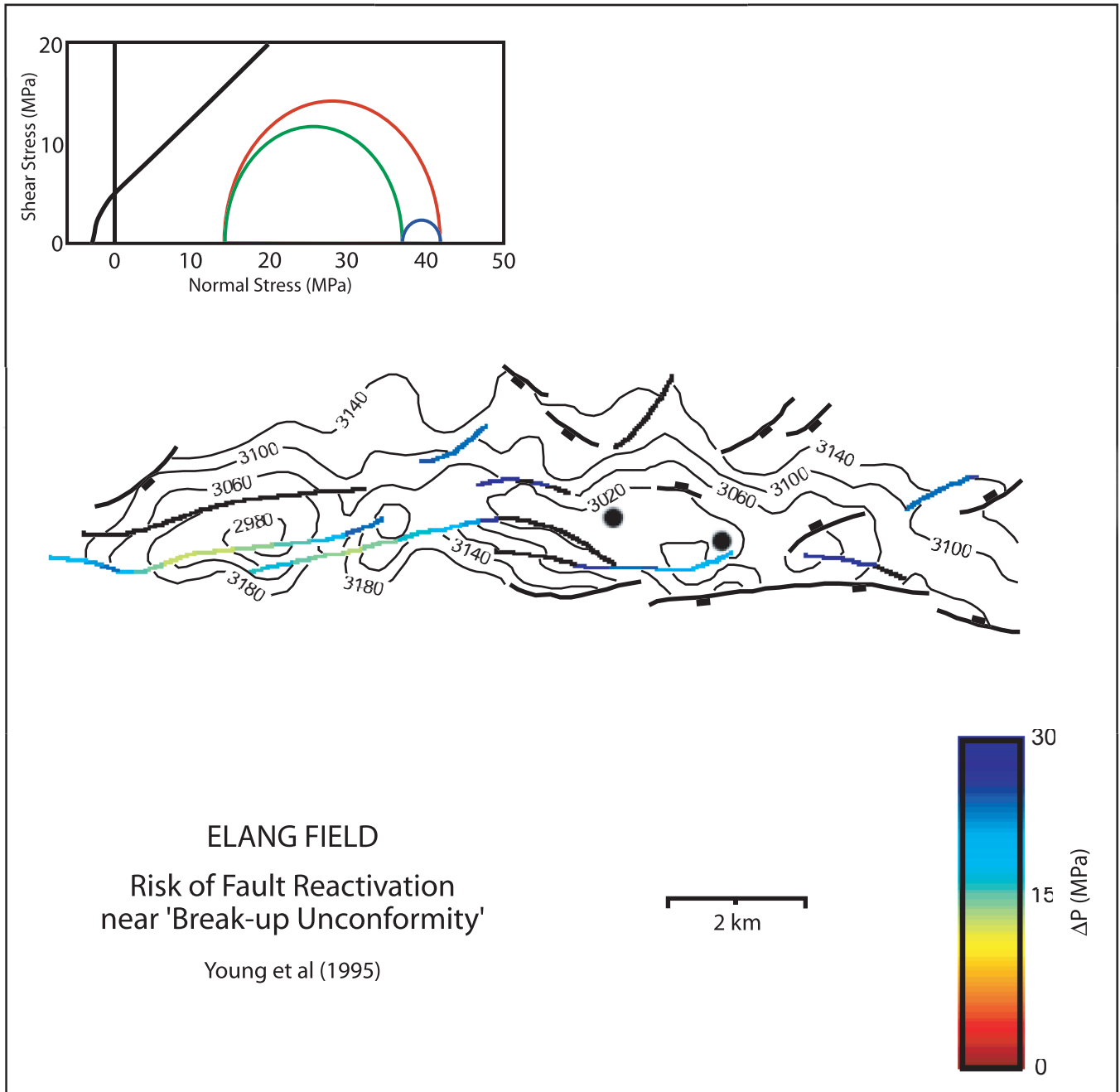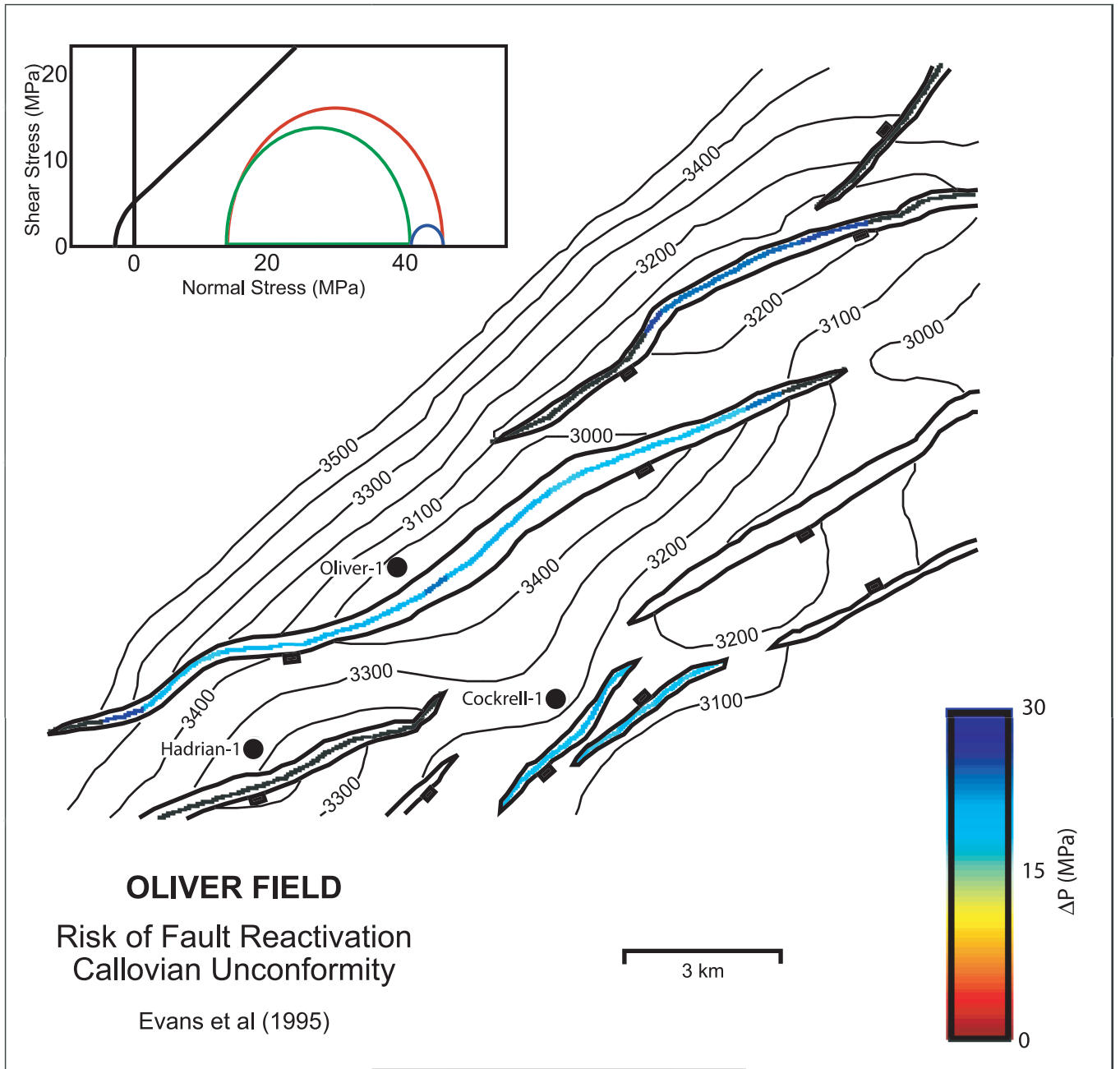
Figure 6. Predicted risk of fault reactivation for the East Swan Prospect measured by ΔP in MPa. Three-dimensional Mohr circle (Figure insert) represents stress environment at 1,750 m depth using generalised Timor Sea stress tensor.

Figure 7. Predicted risk of fault reactivation for the Elang Field measured by ΔP in MPa. Three-dimensional Mohr circle (Figure insert) represents stress environment at 3,000 m depth using generalised Timor Sea stress tensor. Note, where risk colour becomes black, ΔP > 30 MPa.

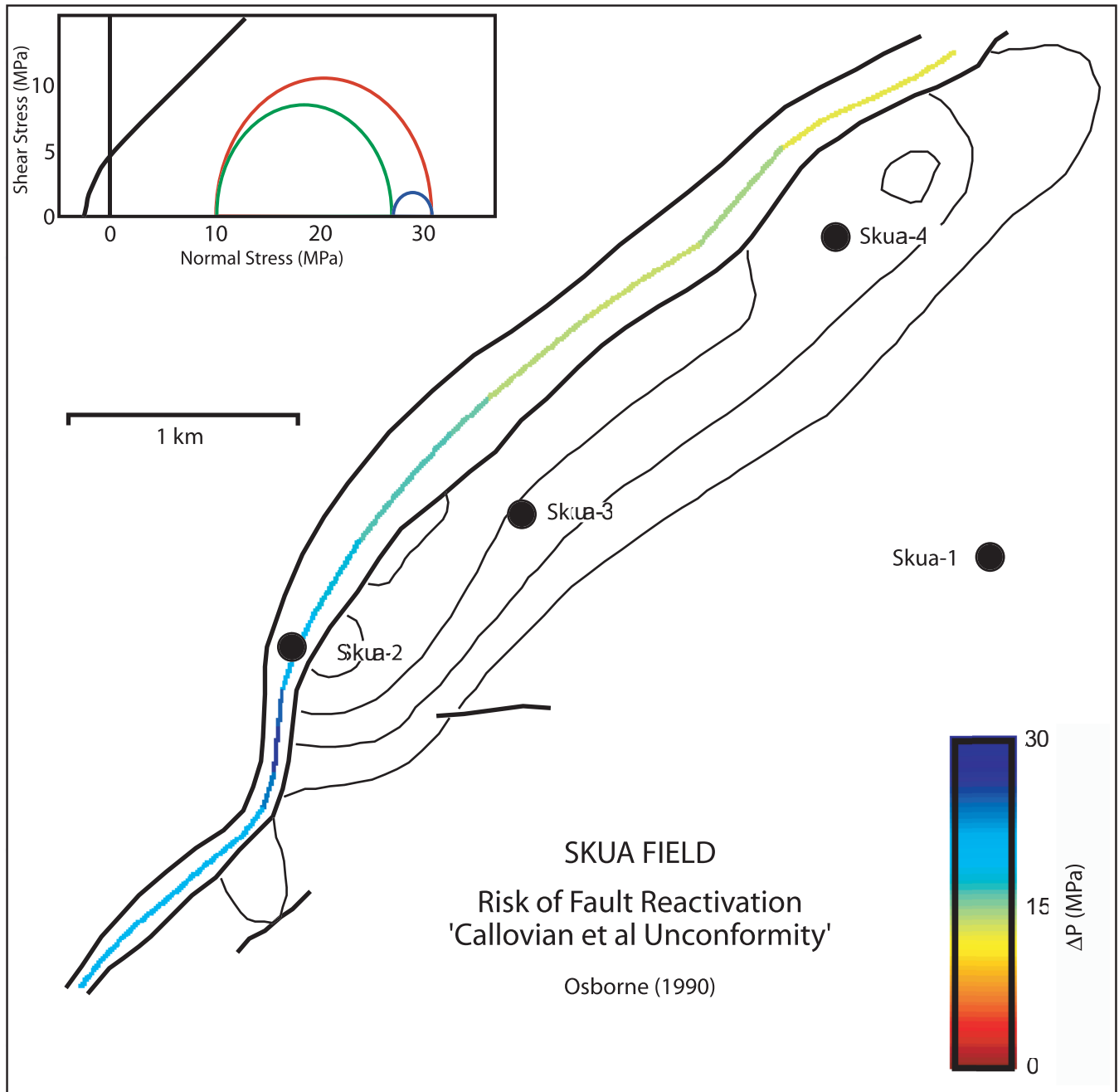**Figure 8.** Predicted risk of fault reactivation for the Oliver Field measured by ΔP in MPa. Three-dimensional Mohr circle (Figure insert) represents stress environment at 3,300 m depth using generalised Timor Sea stress tensor. Note, where risk colour becomes black, ΔP > 30 MPa.
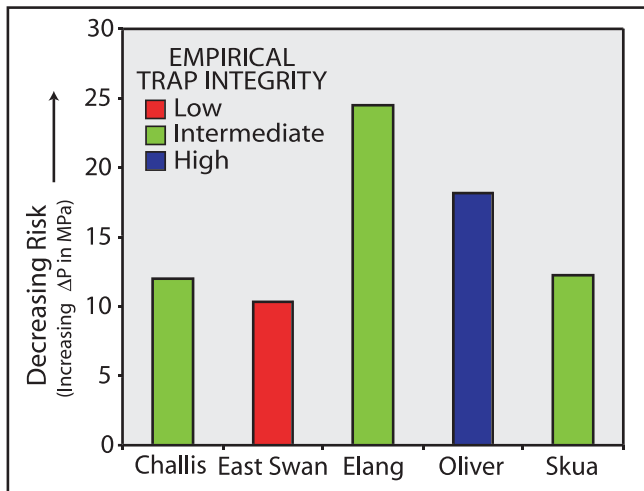
Figure 9. Predicted risk of fault reactivation for the Skua Field measured by ΔP in MPa. Three-dimensional Mohr circle (Figure insert) represents stress environment at 2,300 m depth using generalised Timor Sea stress tensor.

Figure 10. Comparison of empirical trap integrity with predicted fault reactivation risk. Fault reactivation risk is an average of the maximum risk for each individual bounding fault of a trap.

evidence, however, that leakage is occurring at the present day.

The very low risk predicted for Elang suggests that present day leakage may not be occurring. Measurements of contemporary hydrocarbon leakage using ALF or sniffer might be expected to give a negative result at Elang.

The predicted risk at Challis and Skua indicates that there may be a relatively minor difference between conditions required for a low integrity trap and a moderate integrity trap. Structural geometry variation is the most likely influence given that a generalised stress tensor was used in all predictions. The generic risk stereonet (Fig. 3) indicates that fault strike can vary by as much as 60° and still maintain relatively low ΔP values (high risk) for dips >50°. However, ΔP can alter by as much as 15 MPa with only a change in dip magnitude of 10°. Dip magnitudes for both the Challis and Skua traps predominantly range between 40° and 55°, whereas dip magnitudes reach up to 63° along the East Swan bounding fault. It is possible that this difference in dip magnitude is enough to separate a moderate integrity trap from a low integrity trap.

Shear failure has long been considered the dominant mechanism for failure in the Bonaparte Basin (Castillo et al, 1998; Hillis, 1998; De Ruig et al, 2000) and in a stress environment on the boundary of strike-slip and extension, 60° dipping fault planes are critically oriented for shear failure when striking sub-parallel to the σ_{Hmax} orientation.

CONCLUSIONS

Good correlation exists between observed fault trap integrity and fault reactivation predictions made using the FAST methodology. Using a generalised stress tensor and failure envelope:

Low integrity traps are calibrated to a ΔP estimate of 10 MPa or less.

Moderate integrity traps correspond to ΔP values between 10 and 15 MPa.

High integrity traps correspond to ΔP values greater than 15 MPa.

These data can be used as a guide to quickly assess the impact that dynamic fault breach mechanisms may have on hydrocarbon plays prior to drilling. Where detailed stress and structural information are available, FAST analyses performed on individual fault planes is recommended.

These results also highlight the importance that dip magnitude plays in controlling fault reactivation in the Bonaparte Basin and confirms shear failure to be the most likely mode of failure. The dynamic in situ stress environment is an important control on hydrocarbon leakage in the Timor Sea.

ACKNOWLEDGEMENTS

REFERENCES

BALCH, A.H., AND LEE, M.W., 1984—Vertical seismic profiling: techniques, applications and case histories, Boston, International Human Resource Development Corporation, 488.

BARTON, C.A., ZOBACK, M.D., AND MOOS, D., 1995—Fluid flow aong potentially active faults in crystalline rock, Geology, 23, 683–86.

CASTILLO, D.A., HILLIS, R.R., ASQUITH, K. AND FISCHER, M., 1998—State of stress in the Timor Sea area, based on deep wellbore observations and frictional failure criteria: application to fault-trap integrity. In: Purcell, P.G. and Purcell, R.R. (eds) The Sedimentary Basins of Western Australia 2. Proceedings, PESA, Perth, Western Australia, 325–41.

COWLEY, R., AND O'BRIEN, G.W., 2000—Identification and interpretation of leaking hydrocarbons using seismic data: A comparitive montage of examples from the major fields in Australia's North West Shelf and Gippsland Basin, APPEA Journal, 40 (1), 121–150.

COOPER, G.T., BARNES, C.R., BOURNE, J.D., AND CHANNON, G.J., 1988—Hydrocarbon leakage on the North West Shelf, Australia: New information from the integration of Airborne Laser Fluorosensor (ALF) and structural data, In: Purcell, P.G. and Purcell, R.R. (eds) The Sedimentary Basins of Western Australia 2. Proceedings, PESA, Perth, 255–72.

DE RUIG, M.J., TRUPP, M., BISHOP, D.J., KUEK, D. AND CASTILLO, D.A., 2000—Fault architecture in the Nancar Trough/Laminaria area of the Timor Sea, Northern Australia, APPEA Journal, 40 (1), 173–793.

DEWHURST, D.N., JONES, R.M., HILLIS, R.R, AND MILDREN, S.D., (2002)—Microstructural, petrophysical and geomechanical characterisation of fault rocks from the Carnarvon and Otway Basins. This volume.

FERRILL, D.A., WINTERLE, J., WITTMEYER, G., SIMS, D., COLTON, S, ARMSTRONG, A., AND MORRIS, A.P., 1999—Stressed rock strains groundwater at Yucca Mountain, Nevada, GSA Today, May, 1–8.

HILLIS, R.R., AND WILLIAMS, A.F., 1992—Borehole breakouts and stress analysis in the Timor Sea, In Hurst, A., Griffiths, C.M., and Worthington, P.F. (eds) Geological Applications of Wireline Logs II, GSL Special Publications, 65, 157–68.

HILLIS, R.R., MILDREN, S.D., PIGRAM, C.J. AND WILLOUGHBY, D.R., 1997a—Rotation of horizontal stresses in the Australian North West Continental Shelf due to the collision of the Indo-Australian and Eurasian Plates, Tectonics, 16, 323–35.

HILLIS, R.R., CROSBY, D.G. AND KHURANA, A.K., 1997b—A modified fracture gradient relation and its application to East Texas and the Timor Sea. APPEA Journal, 37 (1), 536–45.

HILLIS, R.R., 1998—Mechanisms of dynamic seal failure in the Timor Sea and Central North Sea. In: Purcell, P.G. and Purcell, R.R. (eds) The Sedimentary Basins of Western Australia 2. Proceedings, PESA Symposium, Perth, 313–24.

HILLIS, R.R. AND REYNOLDS, S.D, 2000—The Australian Stress Map, Journal of the Geological Society, 157, 915–21.

JAEGER, J.C., AND COOK, N., 1961—Fundamentals of rock mechanics, Chapman and Hall, 593.

JONES, R.M., BOULT, P., HILLIS, R.R., MILDREN, S.D. AND KALDI, J., 2000—Integrated hydrocarbon seal evaluation in the Penola Trough, Otway Basin. APPEA Journal, 40 (1), 194–211.

KIVIOR, T., KALDI, J.G., AND LANG S.C., 2002—Seal potential in Cretaceous and Late Jurassic rocks of the Vulcan Sub-basin North West Shelf Australia. This volume.

LISK, M., BRINCAT, M.P., EADINGTON, P.J. AND O'BRIEN, G.W., 1998—Hydrocarbon charge in the Vulcan Sub-basin. In n: Purcell, P.G. and Purcell, R.R. (eds.) The Sedimentary Basins of Western Australia 2, Proceedings, PESA Symposium, Perth, 288–302.

LISK, M. AND EADINGTON, P., 1994—Oil migration in the Cartier trough, Vulcan Sub-basin. In: Purcell, P.G. and Purcell, R.R. (eds.) The Sedimentary Basins of Western Australia, Proceedings, PESA Symposium, Perth, 1994, 301–12.

MARTIN, B.A., AND CAWLEY, S.J, 1991—Onshore and offshore petroleum seepage: contrasting a conventional study in Papua New Guinea and airborne laser fluorosensing over the Arafura Sea, APPEA Journal, 31 (1), 333–53.

McGARR, A., AND GAY, N.C., 1978—State of stress in the Earth's crust, Annual Review of Earth and Planetary Sciences, 6, 405-436.

MILDREN, S.D., HILLIS, R.R., FETT, T., AND ROBINSON, P.H., 1994—Contemporary stresses in the Timor Sea: implications for fault-trap integrity, In: Purcell, P.G. and Purcell, R.R. (eds) The Sedimentary Basins of Western Australia, Proceedings, PESA Symposium, Perth, 1994, 301–12.

MILDREN, S.D. AND HILLIS, R.R., 2000—In situ stresses in the southern Bonaparte Basin, Australia: Implications for first- and second-order controls on stress orientation, Geophysical Research Letters, 27, No. 20, 3413–16.

O'BRIEN, G.W., BICKFORD, G., BISHOP, J., HEGGIE, D.T. AND MARSHALL, J.F., 1992—Light Hydrocarbon geochemistry of the Vulcan Sub-basin, Timor Sea: Rig Seismic Survey 97. BMR Record 1992/62.

O'BRIEN, G.W. AND WOODS, E.P., 1995—Hydrocarbon-related diagenetic zones (HRDZs) in the Vulcan Sub-basin, Timor Sea: recognition and exploration implications. APPEA Journal, 35 (1), 220–52.

O'BRIEN G.W., LISK, M., DUDDY, I., EADINGTON, P.J., CADMAN, S. AND FELLOWS, M., 1996—Late Tertiary fluid migration in the Timor Sea: a key control on thermal and diagenetic histories? APPEA Journal, 36 (1), 399–427.

O'BRIEN, G.W., QUAIFE, P., COWLEY, R., MORSE, M., WILSON, D., FELLOWS, M. AND LISK, M., 1998– Evaluating trap integrity in the Vulcan Sub-basin, Timor Sea, Australia, using integrated remote-sensing geochemical technologies. In: Purcell, P.G. and Purcell, R.R. (eds) The Sedimentary Basins of Western Australia 2. Proceedings, PESA Symposium, Perth, 237–54.

OSBORNE, M., 1990—The exploration and appraisal history of the Skua Field, AC/P2 - Timor Sea. APPEA Journal, 30 (1), 27–50.

SERRA, O., 1984—Fundamentals of well-log interpretation, translated from French by P. Westaway and H. Abbott, Development in Petroleum Science, Amsterdam, Elsevier.

SIBSON, R.H., 1996—Structural permeability of fluid-driven fault-fracture meshes. Journal of Structural Geology, 18, 1,031–1042.

SIBSON, R.H., 1998—Conditions for rapid large-volume flow, In Arehart, G.B. and Hulston, J.R. (eds), Water-Rock Interaction: Proceedings, 9th international symposium WRI-9, Taupo, New Zealand, March-April 1998, Balkema, Rotterdam, 35–8.

STREIT, J.E., 1999–Conditions for earthquake surface rupture along the San Andreas fault system, California, Journal of Geophysical Research, 104/B8, 17,929–39.

WATTS, N.L., 1987—Theoretical aspects of cap-rock and fault seals for single- and two-phase hydrocarbon columns. Marine and Petroleum Geology, 4 (1), 274–307.

WHIBLEY, M. AND JACOBSON, T., 1990—Exploration in the northern Bonaparte Basin, Timor Sea WA-199-P, APEA Journal, 30 (1), 7–15.

WORMALD, G.B., 1988—The geology of the Challis Oilfield—Timor Sea, Australia. In: Purcell, P.G. and Purcell, R.R. (eds.) The North West Shelf Australia, Proceedings, PESA Symposium, Perth, 1988, 425–37.

YOUNG, I.F., SCHMEDJE, T.M. AND MUIR, W.F., 1995—The Elang oil discovery establishes a new oil province in the eastern Timor Sea (Timor Gap of Cooperation). APEA Journal, 35 (1), 44–64.

APPEA

Authors' biographies over page.

THE AUTHORS

Scott Mildren is a research fellow at the NCPGG. He completed his PhD at the University of Adelaide in 1997 and took up a position as structural geologist with Z&S (Asia) Ltd (now Baker Atlas Geoscience).At Z&S he interpreted resistivity and acoustic image data with application to in situ stresses and fracture characterisation. His research addresses various petroleum related geomechanical issues such as fault seal integrity, fractured reservoirs and wellbore stability. Member: AAPG, ASEG, PESA and SPE.

Richard Hillis holds the State of South Australia Chair in Petroleum Reservoir Properties/ Petrophysics at the NCPGG, Adelaide University. He graduated BSc (Hons) from Imperial College (London, 1985), and PhD from the University of Edinburgh (1989). After seven years at Adelaide University's Department of Geology and Geophysics, Richard joined the NCPGG in 1999. His main research interests are in petroleum geomechanics and sedimentary basin tectonics. He has published about 50 papers, and has consulted to many Australian and international oil companies in these topics. Member: AAPG, AGU, ASEG, EAGE, GSA, GSL, PESA, SEG and SPE.

John Kaldi is Director of the NCPGG in Adelaide. He studied for the Bachelors and Masters degrees in geology at Queens College, City University of New York, and received a PhD from Cambridge University, England. In 1980–1982 Dr Kaldi worked as a research geologist for the Saskatchewan Geological Survey in Regina, Canada, specialising in Mississippian Carbonate reservoirs. Later he was with Shell Canada as a senior research geologist, focussing on production geology in carbonates and then with ARCO in Plano, Texas, as a senior reservoir geologist. Between 1991 and 1997 he was geological specialist/chief development geologist with ARCO, Indonesia, in Jakarta, working mainly on the evaluation of reservoirs, seals and pay. In 1997 Dr. Kaldi joined VICO Indonesia as chief geologist. John's specialities include carbonate sedimentology and diagenesis, seal evaluation, reservoir geology and multi-disciplinary studies, and he has more than 40 publications on these topics.